RESEARCH ARTICLE
DOI: 10.4274/tjh.galenos.2026.93902

Transcriptomic Characterization of TCR-NK Cells Reveals Challenges Associated with CD3ζ Overexpression

TCR-NK Hücrelerinin Transkriptomik Karakterizasyonu, CD3ζ Yüksek İfadesi ile İlişkili Zorlukları Tespit Etmektedir

Sütlü T. et al.: Transcriptomic Analysis of TCR-NK Cells

Tolga Sütlü[1,2,3], Elif Çelik[3], Betül Çakıcı[2], Serra Özarı[4], Mertkaya Aras[5]
[1]Acıbadem University Faculty of Engineering and Natural Sciences, Department of Molecular Biology and Genetics, İstanbul, Türkiye
[2]Acıbadem University Graduate School of Natural and Applied Sciences, Department of Molecular Biology and Genetics, İstanbul, Türkiye
[3]Acıbadem University Graduate School of Health Sciences, Department of Translational Medicine, İstanbul, Türkiye
[4]Boğaziçi University Faculty of Science, Department of Molecular Biology and Genetics, İstanbul, Türkiye
[5]Türkiye Cancer Institute, Health Institutes of Türkiye, Ankara, Türkiye

Asst. Prof. Tolga Sütlü, M.D., Acıbadem University Faculty of Engineering and Natural Sciences, Department of Molecular Biology and Genetics; Acıbadem University Graduate School of Natural and Applied Sciences, Department of Molecular Biology and Genetics; cıbadem University Graduate School of Health Sciences, Department of Translational Medicine, İstanbul, Türkiye
tolgasutlu@gmail.com
0000-0002-7813-8734

May 5, 2026
August 20, 2026

Abstract
Objective: TCR-engineered NK cells represent a promising strategy for targeting intracellular tumor antigens while overcoming the risk of TCR alpha/beta chain mispairing inherent to TCR-engineered T cells. Previous work showed that CD3ζ overexpression in TCR-NK cells did not improve antigen-specific cytotoxicity and instead increased non-specific background reactivity. This study aims to investigate the molecular alterations associated with this phenotype by examining the transcriptomic profile of engineered NK-92 cells.
Materials and Methods: Wild-type and genetically modified NK-92 cell lines expressing a tyrosinase-specific TCR in the presence or absence of CD3ζ overexpression were analyzed. Bulk RNA sequencing was followed by differential gene-expression analysis, hierarchical clustering, multidimensional scaling, and pathway enrichment analysis. CD28 surface expression was assessed by flow cytometry, and activation-associated signaling responses were evaluated by western blotting after CD3/CD28 stimulation.
Results: CD3ζ-overexpressing NK-92 cells formed distinct transcriptomic clusters and displayed broader gene expression changes. Expression of CD3δγε alone or in combination with tyrosinase-specific TCR resulted in comparatively limited transcriptional divergence from the empty-vector control, whereas CD3ζ inclusion shifted enriched pathways toward lymphocyte activation, cytotoxicity, and PI3K–AKT-related signaling. CD3ζ-overexpressing cells also exhibited increased CD28 surface expression and altered phosphorylation patterns, most notably involving AKT in response to CD3/CD28 stimulation.
Conclusion: CD3ζ overexpression is not a neutral modification in TCR-NK cell engineering. It is associated with broad transcriptional remodeling and activation-associated signaling changes that may provide a molecular context for the previously observed increase in non-specific activity. These findings support TCR-NK engineering strategies that preserve endogenous CD3ζ regulation while introducing only the missing CD3δγε components required for functional TCR expression.

Keywords: TCR-NK cells, natural killer cells, CD3ζ, T cell receptor, transcriptomics, RNA sequencing

Özet
Amaç: TCR ile modifiye edilmiş NK hücreleri, aynı yöntemin uygulandığı T hücrelerinde görülebilen yanlış TCR zincir eşleşmesi riskinden kaçınırken, hücre içi tümör antijenlerinin hedeflenmesi için umut vadeden bir strateji sunmaktadır. Önceki çalışmalar, TCR-NK hücrelerinde ekzojen CD3ζ ifadesinin antijen-spesifik aktiviteyi artırmadığını; bunun yerine arka plan reaktivitesini yükselttiğini göstermiştir. Bu çalışmada, genetik olarak modifiye edilmiş NK-92 hücrelerinin transkriptomik profili incelenerek bu fenotiple ilişkili moleküler değişikliklerin araştırılması amaçlanmıştır.
Gereç ve Yöntemler: CD3ζ yüksek ifadesi bulunan veya bulunmayan, tirozinaz-spesifik TCR ifade eden vahşitip ve modifiye edilmiş NK-92 hücre hatları analiz edilmiştir. Bulk RNA dizileme sonrası diferansiyel gen ifade analizi, hiyerarşik kümeleme, çok boyutlu ölçekleme ve yolak zenginleştirme analizleri yapılmıştır. CD28 yüzey ifadesi akan hücre ölçer ile değerlendirilmiş, aktivasyonla ilişkili sinyal yanıtları ise CD3/CD28 uyarımı sonrasında Western blot ile incelenmiştir.
Bulgular: CD3ζ yüksek ifade eden NK-92 hücreleri belirgin transkriptomik kümeler oluşturmuş ve CD3ζ-negatif gruplara kıyasla daha fazla gen ifadesi değişiklikleri göstermiştir. Tirozinaz-spesifik TCR ile birlikte veya tek başına CD3δγε ekspresyonu, boş vektör kontrolüne kıyasla sınırlı düzeyde transkripsiyonel farklılaşmaya yol açarken, CD3ζ'nin eklenmesi, lenfosit aktivasyonu, sitotoksisite ve PI3K–AKT ilişkili sinyal yolaklarında değişikliklere yol açmıştır. CD3ζ yüksek ifade eden hücrelerde ayrıca CD28 yüzey ifadesinin arttığı ve CD3/CD28 uyarımı sonrasında özellikle AKT ilişkili sinyal paternlerinin değiştiği gözlenmiştir.
Sonuç: CD3ζ aşırı ifadesi, TCR-NK hücre mühendisliğinde nötr bir modifikasyon değildir. Bu durum, geniş çaplı transkripsiyonel yeniden yapılanma ve aktivasyona yönelik sinyal değişiklikleri ile ilişkili olup, bu değişiklikler daha önce gözlenen non-spesifik aktivite artışına moleküler bir bağlam sağlayabilir. Bu bulgular, fonksiyonel TCR ifadesi için gerekli olan CD3δγε bileşenlerini eklerken endojen CD3ζ ifadesiyle yetinen TCR-NK tasarımlarını ön plana çıkartmaktadır.
Anahtar kelimeler: TCR-NK hücreleri, doğal öldürücü hücreler, CD3ζ, T hücresi reseptörü, transkriptomik, RNA dizileme

Introduction
Over the past decade, the field of cancer immunotherapy has emerged as a major therapeutic approach with genetically engineered cytotoxic lymphocytes, particularly T and NK cells, driving the development of targeted cancer treatments. Among these, chimeric antigen receptor (CAR)- and T cell receptor (TCR)- based therapies offer highly powerful but distinct modes of tumor recognition. CARs recognize surface antigens independently of major histocompatibility complex (MHC) molecules, whereas TCRs detect peptides derived from intracellular antigens presented in complex with MHC molecules on the cell surface. This enables TCR-based therapies to target a broad range of tumor-associated antigens and neoantigens that are inaccessible to CAR-mediated targeting [1–3].
A major limitation of TCR-engineered T cells is the well-established risk of TCR chain mispairing. Due to the heterodimeric structure of TCR recognition domain, introduced TCR chains may cross-pair with endogenously expressed TCR chains which may potentially lead to generation of aberrant TCR heterodimers with unpredictable antigen specificity, reduced efficacy, or unwanted autoreactivity [4, 5]. Natural killer (NK) cells provide an alternative platform for TCR engineering because they lack endogenous TCRα/β expression and therefore avoid this problem [6]. NK cells also possess intrinsic antitumor activity and favorable properties for allogeneic cell therapy [7, 8]. Although NK and T cells rely on distinct target-recognition mechanisms, their intracellular activation pathways partially converge on shared signaling events that promote cytotoxic responses and target-cell killing [9, 10].
Previous studies have shown that NK cells can be redirected toward peptide–MHC complexes through the introduction of tumor-specific TCRs together with the required CD3 complex components. Mensali et al. demonstrated antigen-specific recognition by TCR-engineered NK cells, while Parlar et al. showed that NK-92 cells expressing a tyrosinase-specific TCR together with CD3δ, CD3γ, and CD3ε selectively recognize antigen-positive target cells and mediate antigen-specific cytotoxicity [11, 12].
The decision to include CD3ζ in TCR-NK designs appears to be a critical consideration for optimizing NK-cell based TCR therapies. In T cells, CD3ζ is a core signaling component of the TCR/CD3 complex [13]. NK cells also readily express endogenous CD3ζ, where it contributes to signaling downstream of activating receptors such as CD16, NKp30, and NKp46 [9, 14, 15]. In our previous work, we have shown that ectopic CD3ζ expression in TCR-NK cells did not enhance antigen-specific triggering and instead increased background reactivity against antigen-negative target cells [12]. This finding suggested that CD3ζ overexpression is not simply redundant in NK cells but may disturb signaling regulation and compromise the functional specificity of engineered TCR-NK cells. Yet, it still remains unknown whether CD3ζ overexpression primarily affects TCR-associated signaling, broader NK-cell activation pathways, transcriptional activation states, or co-stimulatory receptor expression.
In this study, we aimed to characterize the molecular alterations associated with this unexpected phenotype. We hypothesize that ectopic CD3ζ expression would be associated with broader activation-related transcriptional and

signaling changes beyond those caused by CD3δγε/TCR expression alone. Through bulk RNA sequencing, pathway analysis, flow cytometric validation, and signaling analysis, we examined how CD3ζ overexpression is associated with the transcriptional and activation-associated profile of genetically modified NK-92 cells. Our findings identify broad molecular alterations linked to immune signaling and cellular activation, providing a mechanistic framework for interpreting the previously observed increase in non-specific activity. These results support a more rational TCR-NK engineering strategy in which endogenous CD3ζ regulation is preserved rather than amplified through vector design.

Materials & Methods

Cell Lines and Culture Conditions

Wild type and genetically modified NK-92 (ATCC® CRL-2407™) cells were maintained in complete NK medium consisting of RPMI-1640 supplemented with 20% heat-inactivated fetal bovine serum, 2 mM L-glutamine, 1 mM sodium pyruvate, 0.1 mM MEM non-essential amino acids, 25 mM HEPES, 1× MEM vitamins, 0.1 mM 2-mercaptoethanol, and 1000 U/ml recombinant human IL-2. Cells were cultured at 37°C in a humidified incubator containing 5% CO_2 and maintained at densities between 3×10^5 and 1×10^6 cells/ml.

Genetically Engineered NK-92 Cell Lines

Genetically modified NK-92 cell lines used in this study were generated as previously described by Parlar et al. [12]. The NK-92 cell lines included in this study were as follows: NK-92.wT, unmodified wild-type NK-92 cells; NK-92.iT2puro, control cells expressing tdTomato fluorescent protein and puromycin resistance gene; NK-92.DGEiT2puro, cells expressing CD3δ, CD3γ, and CD3ε along with tdTomato fluorescent protein and puromycin resistance gene; NK-92.DGEZiT2puro, cells expressing CD3δ, CD3γ, CD3ε, and CD3ζ along with tdTomato fluorescent protein and puromycin resistance gene; NK-92.DGE+TYR, cells expressing the tyrosinase-specific TCR together with CD3δ, CD3γ, and CD3ε along with tdTomato fluorescent protein and puromycin resistance gene; and NK-92.DGEZ+TYR, cells expressing the tyrosinase-specific TCR together with CD3δ, CD3γ, CD3ε, and CD3ζ along with tdTomato fluorescent protein and puromycin resistance gene.

RNA Isolation and Bulk RNA Sequencing

Wild-type and genetically modified NK-92 cells were synchronized prior to RNA isolation to minimize potential differences in gene expression associated with variable growth rates. A total of six NK-92 cell lines were sub-cultured every two days at a density of 3.5×10^5 cells/ml for two weeks. RNA isolation was performed in four independent batches. Between each isolation batch, cells were sub-cultured at least twice. For RNA-sequencing, three independent experimental replicates with the highest RNA quality were analyzed for each NK-92 cell line, with replicate samples obtained from separate culture and RNA-isolation batches. The genetically engineered NK-92 cell lines themselves were previously established as described by Parlar *et al.* [12] and were not independently re-generated for the present study. One day before RNA isolation, cells were seeded in 7 ml complete NK medium at a density of 5×10^5 cells/ml. On the day of isolation, 3×10^6 cells were collected, washed once with PBS, and total RNA was isolated using the NucleoSpin® RNA Isolation Kit (Macherey-Nagel, Düren, Germany) according to the manufacturer's protocol.

RNA concentration, purity, and integrity were assessed using a NanoDrop spectrophotometer and BioAnalyzer-based capillary electrophoresis. Eighteen samples, comprising three experimental replicates for each NK-92 cell line, were selected for RNA sequencing based on RIN values and visual inspection of the corresponding BioAnalyzer electropherograms. The RIN values of the selected samples ranged from 8.3 to 9.9, with a mean RIN of approximately 9.6. Library preparation was carried out using the Illumina Stranded mRNA Prep Kit (Illumina, San Diego, CA, USA), followed by paired-end sequencing with a read length of 2 × 150 bp and a target depth of approximately 30 million reads per sample.

Bulk RNA Sequencing Data Analysis

Raw sequencing reads were assessed using FastQC, and adapter sequences and low-quality bases were removed using Trimmomatic [16]. Processed reads were aligned to the updated Homo sapiens hg38 reference genome using HISAT2 [17], with gene, exon, and transcript annotations obtained from the Ensembl database. Gene-level read counts were generated using featureCounts from the Subread package [18]. Based on the retained gene-level count matrices, the number of reads assigned to annotated genes ranged from approximately 17.7 to 22.5 million per sample, with a mean of approximately 20.6 million. Genes with low or absent expressions across samples were filtered out, and the remaining dataset was normalized using the edgeR package in R [19].

The filtered and normalized dataset was used for downstream transcriptomic analyses. Hierarchical clustering of samples was performed using Euclidean distances calculated from normalized read counts, followed by clustering with the Ward.D2 method. Differentially expressed genes were identified using the limma package in R [20], and statistical analyses were performed using R scripts. Differentially expressed genes were defined using thresholds of $|\log2FC| > 0.5$ and $FDR < 0.05$. To assess the robustness of the observed differential-expression patterns, the analysis was additionally evaluated using a more stringent threshold of $|\log2FC| > 1$ and $FDR < 0.05$.

To assess the consistency of CD3ζ-associated transcriptional changes in the presence and absence of TCR expression, gene-level log2FC values from the matched NK-92.DGEiT2puro vs. NK-92.DGEZiT2puro and NK-

92.DGE+TYR vs. NK-92.DGEZ+TYR comparisons were plotted against each other across all analyzed genes. The analysis was additionally performed after restricting the dataset to genes annotated as encoding cell-surface proteins based on Gene Ontology (GO) annotations obtained through the PANTHER Classification System. Pathway enrichment analysis was performed using the Kyoto Encyclopedia of Genes and Genomes (KEGG) PATHWAY database and the clusterProfiler::enrichKEGG package. Upregulated genes were used as input. Pathways were statistically evaluated according to the number of differentially expressed genes assigned to each pathway, and adjusted p values were calculated using the Benjamini–Hochberg correction.

Flow Cytometry Analysis

Cell surface CD28 expression was evaluated in genetically modified NK-92 cell lines by flow cytometry. Surface staining was performed using APC-conjugated anti-human CD28 antibody (clone CD28.2; BD Biosciences, USA), with the corresponding isotype control used to define background staining. Stained cells were acquired by flow cytometry, and data were analyzed using FlowJo software (BD Biosciences, USA). CD28 surface expression was reported as the ratio of CD28 mean fluorescence intensity to isotype control mean fluorescence intensity.

Western Blot Analysis

TCR-expressing NK-92 cells with or without CD3ζ overexpression were analyzed by western blotting following CD3/CD28 stimulation. One day before the experiment, cells were seeded at a concentration of 5×10^5 cells/ml. On the day of stimulation, cells were adjusted to 2×10^5 cells in 100 µl of complete NK medium without FBS and serum-starved for 2 h at 37°C and 5% CO_2. Cells were then stimulated for 30 min with CD3/CD28 beads (Miltenyi Biotec, T Cell TransAct™) at 0.01X, 0.1X, or 1X of the manufacturer's recommended concentration. Following stimulation, cells were lysed in RIPA buffer supplemented with protease and phosphatase inhibitors. Protein lysates were resolved by SDS-PAGE, transferred onto PVDF membranes, and probed with the following primary antibodies: rabbit anti-phospho-AKT [Ser473] (Cell Signaling Technology, #4060, 1:1000), rabbit anti-phospho-AKT [Thr308] (Cell Signaling Technology, #2965, 1:1000), rabbit anti-phospho-p44/42 MAPK/ERK1/2 [Thr202/Tyr204] (Cell Signaling Technology, #9101, 1:1000), rabbit anti-phospho-LCK [Tyr505] (Cell Signaling Technology, #2751, 1:1000), rabbit anti-phospho-PLCγ1 [Tyr783] (Cell Signaling Technology, #2821, 1:1000), rabbit anti-phospho-PKCθ [Thr538] (Cell Signaling Technology, #9377, 1:1000), and rabbit anti-β-actin (Cell Signaling Technology, #4967, 1:1000) as a loading control. Membranes were subsequently incubated with goat anti-rabbit IgG HRP-linked secondary antibody (Cell Signaling Technology, #7074, 1:5000). Signals were visualized using chemiluminescent substrates on a Syngene G:BOX Chemi XRQ system. Band intensities were quantified using ImageJ and normalized to β-actin.

Statistical Analysis

Graphs were prepared and statistical analyses were performed using GraphPad Prism (GraphPad Software Inc., La Jolla, CA, USA).

Results

CD3ζ Overexpression Defines a Distinct Transcriptomic Profile in Genetically Modified NK-92 Cells

Bulk RNA sequencing was performed across six NK-92 cell lines, with three independent samples analyzed per group. Unsupervised multidimensional scaling analysis showed close clustering of replicate samples within each cell line and clear separation of genetically modified NK-92 cells according to their engineering strategy (**Figure 1A**). Wild-type NK-92 cells formed a distinct cluster, while cell lines carrying additional CD3ζ expression separated from both the empty-vector control and the corresponding non-CD3ζ-modified groups. A similar pattern was observed by hierarchical clustering and heatmap analysis of the top 50 most variable transcripts, in which CD3ζ-overexpressing cell lines displayed a distinct expression profile relative to the other genetically modified NK-92 populations (**Figure 1B–C**).

To further assess how altered gene sets were distributed across engineering strategies, Venn diagram analyses were performed in selected comparisons with either wild-type NK-92 cells or the empty-vector NK-92.iT2puro control (**Figure 1D**). In comparisons with wild-type NK-92 cells, non-CD3ζ-engineered groups retained a greater degree of overlap with the empty-vector control, whereas CD3ζ-overexpressing groups displayed a more distinct differential gene-expression pattern. This pattern was even clearer when comparisons were made against NK-92.iT2puro. CD3ζ-containing cell lines revealed a more extensive alteration in their gene expression profile compared to the corresponding non-CD3ζ groups. To evaluate whether these observations were dependent on the relatively permissive |log2FC| threshold used for the primary analysis, we additionally repeated the differential expression analysis using a more stringent cutoff of $|\log2FC| > 1$ and FDR < 0.05. As expected, application of this threshold reduced the overall number of differentially expressed genes. However, the relative pattern across the experimental groups remained consistent with that observed using the $|\log2FC| > 0.5$ cutoff. In particular, comparisons involving CD3ζ-expressing cells continued to show more pronounced transcriptional alterations, whereas changes associated with TCR introduction in the absence of CD3ζ remained comparatively limited. These results are presented in **Supplementary Figure 1** and further support the robustness of the overall transcriptional pattern observed across the different engineering strategies.

To directly assess whether CD3ζ overexpression was associated with similar transcriptional changes in the presence and absence of the TCR, gene-level log2FC values were compared between the matched NK-92.DGEiT2puro vs. NK-92.DGEZiT2puro and NK-92.DGE+TYR vs. NK-92.DGEZ+TYR contrasts (Figure 1E). Across all analyzed genes, the two comparisons showed a concordant pattern in the direction and magnitude of gene-expression changes. A similar pattern was observed when the analysis was restricted to genes encoding cell-surface proteins (Figure 1F). These findings indicate that the transcriptional changes associated with CD3ζ overexpression are largely maintained irrespective of TCR co-expression.

Together, these analyses indicate that the introduction of CD3δγε and TCR has a comparatively limited effect on the overall transcriptomic profile relative to the empty-vector control, while the inclusion of CD3ζ drives a substantially stronger transcriptional shift in engineered NK-92 cells.

CD3ζ Inclusion Broadens Differential Gene Expression Beyond the Effects of Lentiviral Transduction

Whereas the Venn diagram analyses summarized the overall distribution of differentially expressed genes, pairwise comparisons were used to examine the extent of these changes and to distinguish the effects of lentiviral transduction from those of the introduced genetic components (**Table 1 and Supplementary Table S1**). Comparison of NK-92.wT and NK-92.iT2puro cells revealed substantial numbers of both upregulated and downregulated genes, indicating a background transcriptional effect associated with lentiviral vector delivery. Accordingly, all genetically modified cell lines also showed broad gene-expression differences when compared to wild-type NK-92 cells.

To evaluate transcriptional changes beyond effects attributable to lentiviral transduction, engineered NK-92 cell lines were compared directly with the NK-92.iT2puro control. In these comparisons, expression of CD3δγε, either alone or together with the tyrosinase-specific TCR, resulted in relatively limited numbers of differentially expressed genes. In contrast, inclusion of CD3ζ markedly increased both upregulated and downregulated gene counts. This pattern was also evident in matched comparisons of CD3ζ-native and CD3ζ-overexpressing counterparts, supporting CD3ζ overexpression as the major contributor to the expanded differential gene-expression profile. Notably, the addition of the TCR itself caused only modest changes relative to the effect of CD3ζ. These directional gene-expression differences were subsequently examined at the pathway level using KEGG enrichment analysis.

CD3ζ Inclusion Redirects Upregulated Pathway Enrichment Toward Activation-Related Programs

The differential expression analyses showed that CD3ζ inclusion substantially broadened the transcriptional changes observed in engineered NK-92 cells. To determine whether these altered genes converged on distinct biological programs, KEGG pathway enrichment analysis was performed using upregulated genes from selected pairwise comparisons (**Table 2**).

Comparison of NK-92.iT2puro with NK-92.wT showed that empty-vector transduction was associated with enrichment of pathways largely related to viral infection and innate immune responses. A similar pathway profile was observed in CD3ζ-native engineered cell lines when compared with the empty-vector control, suggesting that expression of CD3δγε, independent of the tyrosinase-specific TCR co-expression, did not markedly shift the pathway landscape beyond this lentiviral transduction-associated background.

In contrast, CD3ζ-containing TCR-NK cells displayed a distinct enrichment pattern. When NK-92.DGEZ+TYR cells were compared with either the empty-vector control or their matched CD3ζ-native counterpart, enriched pathways shifted toward lymphocyte signaling and cytotoxicity-related programs. This pattern was most evident in the direct comparison of NK-92.DGEZ+TYR and NK-92.DGE+TYR. A similar, although not statistically significant trend was observed in the matched non-TCR comparison, where T cell receptor signaling ranked as the top upregulated pathway in NK-92.DGEZiT2puro versus NK-92.DGEiT2puro cells (**Supplementary Table S2**). Together, these findings indicate that CD3ζ inclusion, rather than TCR expression alone, is associated with an activation-related pathway profile in engineered NK-92 cells.

CD3ζ Overexpression Is Associated with Increased CD28 Surface Expression and Altered Activation-Related Signaling

Pathway enrichment analysis identified activation-associated signaling programs in CD3ζ-containing TCR-NK cells, including pathways linked to PI3K–Akt signaling. Since CD28 was among the upregulated genes in CD3ζ-overexpressing NK-92 cells, its surface expression was further examined by flow cytometry. CD28/isotype MFI ratios were increased in NK-92.DGEZiT2puro and NK-92.DGEZ+TYR cells relative to their corresponding CD3ζ-native counterparts, confirming that the CD3ζ-associated transcriptional upregulation of CD28 was also reflected at the cell-surface protein level (**Figure 2A**).

To assess whether these alterations were accompanied by changes in activation-associated signaling responses, TCR-expressing NK-92 cells with or without the CD3ζ overexpression were stimulated with increasing concentrations of CD3/CD28 beads and analyzed for activation-associated phosphorylation status of selected signaling proteins. Phosphorylation patterns varied across proteins and stimulation conditions; however, the most apparent CD3ζ-associated differences were observed in AKT phosphorylation, particularly at the highest stimulation concentration. Other phospho-signaling readouts showed more variable or less consistent changes across the tested conditions (**Figure 2B–C**).

Together, these results link CD3ζ-driven transcriptomic remodeling with increased CD28 surface expression and altered responsiveness of activation-associated signaling pathways. Collectively, the transcriptomic, pathway-level, phenotypic, and phospho-signaling findings provide the experimental basis for evaluating how CD3ζ inclusion may reshape engineered TCR-NK cell behavior.

Discussion

This study extends our previous observation that additional CD3ζ expression does not improve antigen-specific TCR-NK cell function but instead increases non-specific background activity [12]. By examining the molecular consequences of CD3ζ overexpression, we show that this phenotype is accompanied by broad transcriptional alterations in activation-associated signaling pathways. These findings suggest that CD3ζ inclusion is not a neutral design parameter in TCR-based NK cell engineering.

A central finding of this study is that the transcriptional impact of TCR-NK engineering depends strongly on the inclusion of CD3ζ. Pathway alterations associated with viral entry and antiviral defense mechanisms were observed across all genetically modified NK-92 cells, likely reflecting the lasting effects of lentiviral gene delivery. However, the introduction of CD3δ, CD3γ, and CD3ε together with the tyrosinase-specific TCR caused only limited divergence from the empty-vector control, whereas the addition of CD3ζ markedly altered the overall expression profile and shifted the affected pathways toward activation-related programs. This indicates that the major transcriptional perturbation is linked specifically to CD3ζ overexpression rather than TCR-NK engineering itself. Since CD3ζ contributes to signaling downstream of activating NK-cell receptors such as CD16, NKp30, and NKp46 [21], its enforced expression may affect broader NK-cell signaling networks beyond the introduced TCR/CD3 complex. These alterations may provide a molecular context for the increased background activity previously observed in CD3ζ-overexpressing TCR-NK cells [12].

Among the altered molecular programs, the CD28/ICOS–PI3K–AKT axis appears particularly relevant. CD3ζ-overexpressing NK-92 cells showed increased expression of genes associated with co-stimulatory and survival-related signaling, including CD28, ICOS, and PI3K-related components, and increased surface CD28 expression was confirmed by flow cytometry. Together with the altered AKT phosphorylation observed following CD3/CD28 stimulation, these findings suggest that CD3ζ overexpression may promote a more activation-permissive state. Because this study does not directly test whether CD28/PI3K–AKT signaling mediates the non-specific cytotoxicity, this pathway should be viewed as a candidate mechanism rather than a confirmed causal driver. Therefore, the present data do not establish a direct causal relationship between this signaling profile and the increase in non-specific activity, and further studies will be required to clarify this connection.

These findings have direct implications for rational TCR-NK cell design. Since endogenous CD3ζ appears sufficient to support TCR function when CD3δ, CD3γ, and CD3ε are introduced, additional CD3ζ expression may be unnecessary. Moreover, the increased background reactivity previously observed following CD3ζ overexpression raises concerns regarding the functional specificity of such designs. This is consistent with the broader view that receptor architecture and signaling components should be uniquely tailored to NK-cell biology rather than directly adopted from T-cell platforms [22]. Our results therefore support TCR-NK designs that preserve endogenous CD3ζ regulation while introducing only the missing CD3δγε components required for functional TCR expression.

This study also addresses a relatively underexplored aspect of CD3ζ biology. While CD3ζ downregulation has long been associated with impaired lymphocyte responsiveness in cancer and chronic immune dysfunction [23], far less is known about the consequences of CD3ζ upregulation or enforced overexpression, particularly in NK cells. Our findings suggest that increased CD3ζ abundance can reshape the transcriptional and signaling profile of engineered NK cells, highlighting CD3ζ dosage as a relevant variable in receptor-modified NK-cell platforms.

Several limitations regarding this study should also be considered. First, the study was conducted exclusively in NK-92 cells. Although this model provides a controlled background in which the transcriptional consequences of individual engineering components can be compared, NK-92 cells differ from primary human NK cells in their differentiation state, receptor repertoire, and signaling characteristics. Consequently, the extent to which CD3ζ overexpression induces similar transcriptional remodeling in primary NK cells remains unknown. Future studies using primary NK cells from multiple healthy donors, and ultimately patient-derived NK cells, combining transcriptomic profiling with functional assessment following TCR/CD3 engineering will therefore be necessary to establish the generalizability and translational relevance of these findings. This is particularly important because NK-92-based products have additional clinical considerations, including the requirement for irradiation before infusion [24]. Second, bulk transcriptomic profiling provides an average view of gene expression across each engineered population and may not capture cell-to-cell variation in transgene expression or signaling states arising from lentiviral modification. Third, further experiments are needed to define the specific contribution of the CD28/ICOS–PI3K–AKT axis to the background activity associated with CD3ζ overexpression.

Although increased background reactivity associated with CD3ζ overexpression was demonstrated previously using this TCR-NK-92 model [12], the present study did not directly test whether the transcriptional and signaling alterations identified here are causally responsible for this functional phenotype. Accordingly, these molecular findings should be interpreted as a mechanistic framework associated with, rather than a direct

demonstration of the cause of nonspecific cytotoxicity. Future studies combining targeted perturbation of candidate pathways with antigen-specific and antigen-independent cytotoxicity assays will be required to establish such causal relationships.

In conclusion, this study provides a molecular framework for understanding why CD3ζ inclusion may be unfavorable in TCR-NK engineering. CD3ζ overexpression was associated with broad transcriptional remodeling and altered activation-related signaling that may contribute to increased non-specific activity. These findings support TCR-NK cell designs that rely on endogenous CD3ζ and introduce only the missing CD3δγε components, which may help preserve antigen specificity while minimizing unnecessary perturbation of NK-cell signaling networks.

Financial Disclosure Statement:
This study was supported by TUBİTAK grant number 218S897

Conflict-of-interest Statement:
T.S. is an inventor on US Patent US11752172B2 and a founding shareholder in Vycellix Inc.

References

1. Pardoll D and Drake C. Immunotherapy earns its spot in the ranks of cancer therapy. J Exp Med. 2012;209(2):201–9.
2. Shafer P, Kelly LM, and Hoyos V. Cancer Therapy With TCR-Engineered T Cells: Current Strategies, Challenges, and Prospects. Front Immunol. 2022;13.
3. Brudno JN, Maus M V., and Hinrichs CS. CAR T Cells and T-Cell Therapies for Cancer: A Translational Science Review. JAMA. 2024;332(22):1924–35.
4. Bendle GM, Linnemann C, Hooijkaas AI, Bies L, De Witte MA, Jorritsma A, Kaiser ADM, Pouw N, Debets R, Kieback E, et al. Lethal graft-versus-host disease in mouse models of T cell receptor gene therapy. Nat Med. 2010;16(5):565–70.
5. Van Loenen MM, De Boer R, Amir AL, Hagedoorn RS, Volbeda GL, Willemze R, Van Rood JJ, Falkenburg JHF, and Heemskerk MHM. Mixed T cell receptor dimers harbor potentially harmful neoreactivity. Proc Natl Acad Sci U S A. 2010;107(24):10972–7.
6. Karahan ZS, Aras M, and Sütlü T. TCR-NK Cells: A Novel Source for Adoptive Immunotherapy of Cancer. Turkish Journal of Hematology. 2023;40(1):1–10.
7. Lanier LL. Up on the tightrope: natural killer cell activation and inhibition. Nat Immunol. 2008;9(5):495–502.
8. McCurdy SR. Harnessing allogeneic NK cells: improving outcomes with tailored donor lymphocyte infusion. J Clin Invest. 2022;132(11).
9. Tomasello E, Blery M, Vely E, and Vivier E. Signaling pathways engaged by NK cell receptors: Double concerto for activating receptors, inhibitory receptors and NK cells. Semin Immunol. 2000;12(2):139–47.
10. Shah K, Al-Haidari A, Sun J, and Kazi JU. T cell receptor (TCR) signaling in health and disease. Signal Transduction and Targeted Therapy 2021 6:1. 2021;6(1):412-.
11. Mensali N, Dillard P, Hebeisen M, Lorenz S, Theodossiou T, Myhre MR, Fåne A, Gaudernack G, Kvalheim G, Myklebust JH, et al. NK cells specifically TCR-dressed to kill cancer cells. EBioMedicine. 2019;40:106–17.
12. Parlar A, Sayitoglu EC, Ozkazanc D, Georgoudaki AM, Pamukcu C, Aras M, Josey BJ, Chrobok M, Branecki S, Zahedimaram P, et al. Engineering antigen-specific NK cell lines against the melanoma-associated antigen tyrosinase via TCR gene transfer. Eur J Immunol. 2019;49(8):1278–90.
13. Love PE and Hayes SM. ITAM-mediated signaling by the T-cell antigen receptor. Cold Spring Harb Perspect Biol. 2010;2(6).
14. Anderson P, Caligiuri M, Ritz J, and Schlossman SF. CD3-negative natural killer cells express zeta TCR as part of a novel molecular complex. Nature. 1989;341(6238):159–62.
15. Lanier LL, Corliss B, and Phillips JH. Arousal and inhibition of human NK cells. Immunol Rev. 1997;155:145–54.
16. Bolger AM, Lohse M, and Usadel B. Trimmomatic: a flexible trimmer for Illumina sequence data. Bioinformatics. 2014;30(15):2114–20.
17. Kim D, Paggi JM, Park C, Bennett C, and Salzberg SL. Graph-based genome alignment and genotyping with HISAT2 and HISAT-genotype. Nat Biotechnol. 2019;37(8):907–15.
18. Liao Y, Smyth GK, and Shi W. The R package Rsubread is easier, faster, cheaper and better for alignment and quantification of RNA sequencing reads. Nucleic Acids Res. 2019;47(8):e47–e47.
19. Robinson MD, McCarthy DJ, and Smyth GK. edgeR: a Bioconductor package for differential expression analysis of digital gene expression data. Bioinformatics. 2010;26(1):139–40.

20. Ritchie ME, Phipson B, Wu D, Hu Y, Law CW, Shi W, and Smyth GK. limma powers differential expression analyses for RNA-sequencing and microarray studies. Nucleic Acids Res. 2015;43(7):e47–e47.
21. Chen S, Zhu H, and Jounaidi Y. Comprehensive snapshots of natural killer cells functions, signaling, molecular mechanisms and clinical utilization. Signal Transduction and Targeted Therapy 2024 9:1. 2024;9(1):302-.
22. Page A, Chuvin N, Valladeau-Guilemond J, and Depil S. Development of NK cell-based cancer immunotherapies through receptor engineering. Cellular & Molecular Immunology 2024 21:4. 2024;21(4):315–31.
23. Baniyash M. TCR zeta-chain downregulation: curtailing an excessive inflammatory immune response. Nat Rev Immunol. 2004;4(9):675–87.
24. Klingemann H. The NK-92 cell line—30 years later: its impact on natural killer cell research and treatment of cancer. Cytotherapy. 2023;25(5):451–7.

Table 1. Differentially upregulated and downregulated gene counts across pairwise comparisons of NK-92 cell lines. Differentially expressed genes were defined as |log2FC| > 0.5 and FDR < 0.05

Reference Group	Comparison Group	Upregulated Gene Count	Downregulated Gene Count
NK-92.wT	NK-92.iT2puro	244	315
NK-92.wT	NK-92.DGEiT2puro	238	325
NK-92.wT	NK-92.DGEZiT2puro	157	243
NK-92.wT	NK-92.DGE+TYR	209	298
NK-92.wT	NK-92.DGEZ+TYR	178	181
NK-92.iT2puro	NK-92.DGEiT2puro	42	26
NK-92.iT2puro	NK-92.DGEZiT2puro	166	228
NK-92.iT2puro	NK-92.DGE+TYR	45	14
NK-92.iT2puro	NK-92.DGEZ+TYR	221	198
NK-92.DGEiT2puro	NK-92.DGEZiT2puro	166	165
NK-92.DGEiT2puro	NK-92.DGE+TYR	5	3
NK-92.DGEZiT2puro	NK-92.DGEZ+TYR	44	7
NK-92.DGE+TYR	NK-92.DGEZ+TYR	203	185

Table 2. Significantly enriched KEGG pathways across selected pairwise comparisons of NK-92 cell lines. Analyses were performed using clusterProfiler::enrichKEGG with upregulated genes (log2FC > 0.5, FDR < 0.05). Gene Ratio indicates pathway-mapped input genes/total KEGG pathway genes; adjusted p values were Benjamini–Hochberg corrected.

Comparison	KEGG ID	Upregulated KEGG Pathway	Gene Ratio	Adj. P Value
NK-92.iT2puro vs. NK-92.wT	hsa05164	Influenza A	19/171	0
	hsa05169	Epstein-Barr virus infection	20/202	0
	hsa05203	Viral carcinogenesis	18/204	0.00003
	hsa05162	Measles	14/139	0.00009
	hsa04621	NOD-like receptor signaling pathway	16/184	0.00009
NK-92.DGEiT2puro vs. NK-92.iT2puro	hsa04064	NF-kappa B signaling pathway	7/104	0.00088
	hsa05310	Asthma	4/31	0.00340
	hsa04625	C-type lectin receptor signaling pathway	6/104	0.00340
	hsa05145	Toxoplasmosis	6/112	0.00386
	hsa05169	Epstein–Barr virus infection	7/202	0.01143
NK-92.DGE+TYR vs. NK-92.iT2puro	hsa05310	Asthma	5/31	0.00058
	hsa05145	Toxoplasmosis	7/112	0.00196
	hsa04640	Hematopoietic cell lineage	6/99	0.00460
	hsa04064	NF-kappa B signaling pathway	6/104	0.00477
	hsa04514	Cell adhesion molecules	7/157	0.00477
NK-92.DGEZ+TYR vs. NK-92.iT2puro	hsa04514	Cell adhesion molecules	12/157	0.01450
	hsa04660	T cell receptor signaling pathway	9/104	0.02482
	hsa04152	AMPK signaling pathway	9/121	0.03126
	hsa05330	Allograft rejection	5/38	0.03126
	hsa05222	Small cell lung cancer	7/92	0.04580
NK-92.DGEZ+TYR vs. NK-92.DGE+TYR	hsa04660	T cell receptor signaling pathway	12/104	0.00034
	hsa04650	NK cell-mediated cytotoxicity	11/131	0.00978
	hsa04151	PI3K-Akt signaling pathway	19/354	0.00978
	hsa04662	B cell receptor signaling pathway	8/82	0.01762

Supplementary Table S1. Top differentially expressed genes across pairwise comparisons.
For each indicated comparison, the 20 most strongly upregulated and 20 most strongly downregulated differentially expressed genes (DEGs) were selected using thresholds of **|log2FC| > 0.5 and FDR < 0.05**. Genes were ranked according to log2FC within each direction of regulation. For comparisons containing fewer than 20 significant DEGs in either direction, all genes meeting the specified criteria are presented. Gene symbol, rank, log2FC, and FDR-adjusted *p* value are provided for each DEG. For each comparison, positive log2FC values indicate higher expression in the second-listed group relative to the first-listed group, whereas negative log2FC values indicate lower expression in the second-listed group.

Rank	Gene Symbol	log2FC	FDR (adj. P value)
wT vs iT2puro			
1	UGT1A6	8.227	2.13E-06
2	SCHIP1	4.044	3.10E-02
3	IFI44L	3.179	5.83E-04
4	PHLDA1	2.917	1.54E-06
5	IRF5	2.914	7.01E-03
6	RSAD2	2.853	1.54E-06
7	H2BC12	2.825	1.10E-08
8	TNF	2.808	4.05E-07
9	IDUA	2.586	3.16E-05
10	IFIT3	2.585	1.32E-05
11	H2AC6	2.443	6.88E-08
12	H1-2	2.380	2.13E-08
13	H2BC17	2.344	5.87E-07
14	H2BC11	2.267	1.21E-07
15	RP1-34B20	2.259	3.59E-06
16	TMEM273	2.243	5.26E-08
17	XAF1	2.208	5.65E-05
18	DSCR8	2.117	2.08E-05
19	EPSTI1	2.117	3.88E-04
20	LRRN3	2.101	8.30E-09
1	DMKN	-4.754	3.50E-08
2	KIAA0930	-4.592	5.25E-08
3	ADGRG3	-4.252	2.60E-09
4	FGFBP2	-3.998	6.91E-08
5	CEACAM16-AS1	-3.625	1.00E-05
6	FUT7	-3.551	5.07E-05
7	S100A9	-3.111	3.46E-04
8	CDK14	-2.915	3.89E-07
9	AHNAK	-2.890	2.94E-06
10	IL10	-2.733	9.43E-08
11	BCAT1	-2.732	2.73E-06
12	PLXND1	-2.588	2.45E-04
13	MXI1	-2.555	1.24E-06
14	RNF144A	-2.543	4.03E-04

15	C16orf54	-2.530	1.48E-06
16	IGFBP7	-2.517	1.24E-06
17	ITGA6	-2.490	3.07E-07
18	CHI3L1	-2.467	1.14E-02
19	ANXA1	-2.446	7.85E-05
20	ALDH1L1	-2.386	9.54E-05
wT vs DGEiT2p			
1	TLL1	6.079	5.00E-10
2	IGFBP3	5.916	3.50E-09
3	IRF5	5.873	3.50E-09
4	TBXAS1	4.271	6.69E-08
5	SLC39A12	4.047	1.52E-02
6	PHLDA1	3.825	1.01E-08
7	LMNA	3.576	3.47E-06
8	TNF	3.060	9.44E-08
9	H2BC17	3.012	8.90E-09
10	H2BC12	3.001	3.70E-09
11	H2AC6	2.833	4.10E-09
12	H1-2	2.715	3.50E-09
13	LINC00973	2.683	3.75E-07
14	IFI44L	2.644	6.46E-03
15	GLDC	2.537	3.50E-09
16	RSAD2	2.512	1.15E-05
17	FCRL4	2.505	2.12E-07
18	AGRN	2.484	1.04E-04
19	LPAR3	2.440	6.98E-03
20	RP1-34B20	2.231	5.08E-06
1	CDK14	-5.417	2.37E-08
2	RNF144A	-4.785	9.70E-07
3	KIAA0930	-4.224	7.36E-08
4	FGFBP2	-4.211	4.44E-08
5	ALDH1L1	-4.000	4.69E-07
6	CEACAM16-AS1	-3.263	1.58E-05
7	C16orf54	-2.798	2.93E-07
8	AHNAK	-2.701	4.11E-06
9	DUSP23	-2.517	1.37E-08
10	IGFBP7	-2.249	2.37E-06
11	BCAT1	-2.241	3.35E-05
12	RP11-666A1	-2.141	2.09E-03
13	IL10	-2.121	4.63E-07
14	OSBPL5	-2.097	4.48E-08
15	YPEL5	-2.076	6.34E-04
16	RP1-244F24	-2.067	1.58E-05
17	PRDM16	-1.990	1.09E-04
18	RP11-10G12	-1.960	3.61E-02
19	KLF2	-1.934	5.80E-04
20	SLAMF8	-1.900	1.70E-05
wT vs DGEZiT2p			

1	SCHIP1	7.083	8.99E-08
2	OPHN1	6.506	1.00E-10
3	SLC39A12	6.083	2.13E-07
4	PLOD2	5.040	4.38E-08
5	RP11-467L13	4.919	2.44E-02
6	TLL1	4.599	8.01E-05
7	LPAR3	3.796	1.11E-05
8	TNF	3.202	6.98E-08
9	GLDC	2.830	7.00E-10
10	TMEM273	2.309	3.53E-08
11	COL5A2	2.240	1.39E-04
12	PHLDA1	2.158	2.42E-04
13	CCL18	2.073	5.68E-06
14	CD83	1.936	9.26E-06
15	IDUA	1.927	1.53E-02
16	LINC00973	1.884	1.24E-03
17	NPDC1	1.854	2.99E-07
18	H2AC6	1.821	7.67E-06
19	H2BC12	1.799	6.44E-06
20	HLA-DRB5	1.729	3.79E-04
1	RNA5-8SN2	-7.085	2.61E-02
2	FGFBP2	-3.857	1.04E-07
3	AHNAK	-3.780	1.24E-06
4	CEACAM16-AS1	-3.696	1.40E-05
5	PLXND1	-3.510	7.11E-05
6	KIAA0930	-2.976	8.27E-06
7	IL10	-2.573	1.83E-07
8	S100A9	-2.390	1.86E-03
9	CERK	-2.336	1.89E-04
10	TSPAN33	-2.169	6.78E-03
11	C16orf54	-2.058	4.15E-05
12	NDRG1	-2.018	5.47E-07
13	TCAF2	-1.984	1.18E-03
14	IGFBP7	-1.964	9.94E-06
15	PFKFB3	-1.878	1.00E-10
16	H1-10	-1.833	8.90E-05
17	DMKN	-1.798	9.51E-06
18	RP1-244F24	-1.742	2.51E-04
19	ANXA1	-1.662	1.35E-03
20	HLA-DPB1	-1.578	5.22E-04
wT vs DGE+TYR			
1	TRBV10-3	11.461	6.30E-07
2	TRAV4	10.839	3.53E-07
3	TRAJ42	7.901	4.22E-04
4	TRBJ1-3	7.478	1.05E-03
5	TLL1	5.654	5.60E-09
6	IGFBP3	5.348	1.91E-08
7	SLC39A12	3.989	2.21E-02

8	PHLDA1	3.424	1.08E-07
9	IRF5	3.156	2.12E-03
10	IFI44L	3.049	1.29E-03
11	TNF	2.996	1.56E-07
12	TBXAS1	2.834	1.91E-04
13	H2BC12	2.830	1.18E-08
14	H2BC17	2.708	7.12E-08
15	H2AC6	2.680	1.50E-08
16	LPAR3	2.616	3.05E-03
17	RSAD2	2.608	7.31E-06
18	H1-2	2.587	8.30E-09
19	GLDC	2.473	8.30E-09
20	FCRL4	2.435	3.93E-07
1	CDK14	-5.531	3.16E-08
2	KIAA0930	-5.234	1.50E-08
3	RNF144A	-4.995	9.68E-07
4	FGFBP2	-4.409	5.15E-08
5	ALDH1L1	-3.841	7.40E-07
6	CEACAM16-AS1	-3.431	1.49E-05
7	AHNAK	-3.317	1.53E-06
8	C16orf54	-2.806	3.93E-07
9	ITGAX	-2.353	3.97E-03
10	BCAT1	-2.279	3.62E-05
11	IL10	-2.167	5.03E-07
12	IGFBP7	-2.138	4.26E-06
13	DUSP23	-2.107	1.27E-07
14	SLAMF8	-2.049	1.19E-05
15	OSBPL5	-2.047	6.87E-08
16	PRDM16	-1.881	1.96E-04
17	YPEL5	-1.872	2.17E-03
18	ANXA1	-1.854	5.51E-04
19	ITGA6	-1.837	3.16E-06
20	STXBP1	-1.721	1.20E-04
wT vs DGEZ+TYR			
1	TRBV10-3	11.384	1.18E-06
2	TRAV4	10.782	6.38E-07
3	TRAJ42	8.251	2.34E-04
4	TRBJ1-3	7.869	5.36E-04
5	SCHIP1	7.382	2.39E-08
6	SLC39A12	6.048	3.28E-07
7	OPHN1	5.963	8.00E-10
8	PLOD2	5.908	8.00E-10
9	LPAR3	4.432	6.81E-07
10	TLL1	4.068	2.76E-03
11	GLDC	2.812	8.00E-10
12	COL5A2	2.725	7.21E-06
13	TNF	2.365	1.04E-05
14	NPDC1	2.246	1.36E-08

15	IDUA	2.172	2.95E-03
16	H2BC12	2.155	6.81E-07
17	H2AC6	2.057	1.34E-06
18	H2BC17	2.054	7.53E-06
19	CCL18	2.001	8.40E-06
20	LINC00973	1.856	1.83E-03
1	FGFBP2	-3.577	1.65E-07
2	S100A9	-3.449	3.33E-04
3	CERK	-2.985	1.27E-05
4	KIAA0930	-2.686	2.95E-05
5	RP1-244F24	-2.678	8.80E-07
6	AHNAK	-2.626	8.40E-06
7	ANXA1	-2.516	1.02E-04
8	CEACAM16-AS1	-2.481	1.28E-04
9	ADGRG3	-2.394	1.27E-06
10	CD38	-2.357	3.54E-06
11	CHI3L1	-2.120	2.92E-02
12	SPOCK1	-2.037	1.04E-02
13	HLA-DPB1	-2.008	2.49E-05
14	TIE1	-1.940	8.48E-05
15	ITGA6	-1.879	3.66E-06
16	TCAF2	-1.851	2.53E-03
17	PLXND1	-1.826	2.93E-03
18	TSPAN33	-1.824	1.67E-02
19	LGALS3BP	-1.802	5.46E-03
20	PFKFB3	-1.789	4.00E-10
iT2puro vs DGEiT2p			
1	IGFBP3	4.687	6.80E-09
2	TBXAS1	4.621	2.28E-07
3	ADGRG3	4.171	3.40E-09
4	LMNA	3.340	4.09E-05
5	TLL1	3.330	7.00E-09
6	DMKN	3.226	3.61E-04
7	IRF5	2.959	2.28E-07
8	PLXND1	2.915	3.18E-04
9	FUT7	2.696	1.89E-02
10	LINC00973	2.652	2.98E-06
11	PTAFR	2.490	3.40E-09
12	TSPAN33	2.245	1.67E-03
13	LGALS3BP	1.820	5.42E-05
14	NCR2	1.780	2.23E-05
15	ADTRP	1.774	9.25E-03
16	CCL18	1.510	5.70E-04
17	EMP3	1.319	2.23E-05
18	GNLY	1.194	1.17E-04
19	SERPINB9	1.062	4.34E-03
20	GZMH	1.014	5.94E-04
1	UGT1A6	-7.095	2.23E-05

2	TYROBP	-1.548	3.16E-06
3	GIMAP7	-1.535	4.41E-04
4	DUSP23	-1.473	4.21E-02
5	CXXC5	-1.272	3.19E-02
6	RNPEP	-1.270	1.16E-02
7	PLAAT4	-1.104	1.09E-04
8	CEACAM21	-0.939	4.92E-02
9	RGL4	-0.868	2.76E-04
10	PLAAT3	-0.863	1.16E-02
11	LBH	-0.851	3.48E-02
12	VSIR	-0.842	4.40E-02
13	TRAPPC6A	-0.790	2.48E-03
14	ZBP1	-0.721	2.22E-02
15	RP11-79E3	-0.700	7.38E-03
16	CTSZ	-0.660	6.38E-04
17	TCIRG1	-0.625	1.00E-02
18	GSTP1	-0.617	3.32E-05
19	USP28	-0.597	4.95E-02
20	NCAM1	-0.552	2.55E-03
iT2puro vs DGEZiT2p			
1	OPHN1	5.221	2.00E-10
2	PLOD2	3.695	2.47E-07
3	CDK14	3.181	2.27E-07
4	ADGRG3	3.087	2.11E-04
5	SLC39A12	3.081	9.42E-06
6	SCHIP1	3.039	2.02E-06
7	S100A4	2.970	1.10E-04
8	DMKN	2.955	6.90E-04
9	ALDH1L1	2.574	1.61E-05
10	BCAT1	2.463	1.02E-04
11	SMIM24	2.438	4.42E-06
12	FUT7	2.402	1.32E-02
13	NR4A2	2.269	1.21E-04
14	MT1E	2.073	7.80E-04
15	RHOQ	1.986	1.19E-08
16	PTAFR	1.855	3.10E-07
17	LINC00973	1.852	1.36E-03
18	TLL1	1.850	3.22E-02
19	AC144831	1.825	2.62E-05
20	EMP3	1.764	1.05E-07
1	UGT1A6	-8.227	4.62E-06
2	RNA5-8SN2	-7.164	2.12E-02
3	IRF5	-3.095	6.30E-03
4	BCL2A1	-2.770	3.62E-05
5	AGRN	-2.623	2.60E-03
6	H1-10	-2.538	1.11E-06
7	IFI44L	-2.368	3.22E-03
8	RSAD2	-2.249	1.19E-05

9	P2RY8	-2.122	2.53E-05
10	MX1	-1.907	1.43E-03
11	EIF4EBP1	-1.785	6.50E-09
12	IRF7	-1.754	4.96E-04
13	CERK	-1.700	3.01E-02
14	ISG15	-1.692	8.86E-05
15	EPSTI1	-1.652	2.44E-03
16	CMPK2	-1.607	1.35E-06
17	NDRG1	-1.575	1.50E-04
18	RP11-405M12	-1.572	2.33E-06
19	GSDMD	-1.534	1.38E-06
20	MPZL3	-1.528	8.00E-10
iT2puro vs DGE+TYR			
1	TRBV10-3	11.461	5.11E-06
2	TRAV4	10.839	3.52E-06
3	TRAJ42	7.901	3.03E-03
4	TRBJ1-3	7.478	6.33E-03
5	ADGRG3	4.308	1.70E-09
6	IGFBP3	4.120	5.66E-07
7	TBXAS1	3.185	5.10E-04
8	DMKN	3.150	9.30E-04
9	TLL1	2.905	1.91E-05
10	PLXND1	2.192	1.36E-02
11	LMNA	2.161	2.04E-02
12	LGALS3BP	1.947	2.36E-05
13	ADTRP	1.778	8.12E-03
14	SMIM24	1.778	2.10E-02
15	PTAFR	1.695	5.11E-06
16	CCL18	1.551	5.10E-04
17	EMP3	1.344	1.91E-05
18	HLA-DRB5	1.199	2.86E-02
19	HIP1R	1.164	4.56E-02
20	NCR2	1.152	5.56E-03
1	UGT1A6	-8.227	1.96E-05
2	SLC22A18	-1.405	2.16E-02
3	RNPEP	-1.321	8.10E-03
4	GIMAP7	-1.096	5.56E-03
5	CTSZ	-0.910	3.19E-06
6	LBH	-0.902	2.65E-02
7	LZTS1	-0.752	1.48E-02
8	RGL4	-0.745	1.14E-03
9	PLAAT4	-0.710	4.74E-03
10	KRT86	-0.701	3.78E-02
11	CD99	-0.653	2.32E-03
12	CLU	-0.652	7.20E-03
13	TC2N	-0.598	1.36E-02
14	TYROBP	-0.519	2.90E-02
iT2puro vs DGEZ+TYR			

1	TRBV10-3	11.384	1.41E-06
2	TRAV4	10.782	8.53E-07
3	TRAJ42	8.251	2.07E-04
4	TRBJ1-3	7.869	4.50E-04
5	OPHN1	4.678	4.40E-09
6	PLOD2	4.563	4.40E-09
7	DMKN	4.213	8.53E-07
8	SCHIP1	3.339	6.66E-07
9	CDK14	3.134	4.20E-07
10	SLC39A12	3.046	1.21E-05
11	RNF144A	2.976	7.35E-06
12	FUT7	2.785	2.37E-03
13	SMIM24	2.542	2.09E-06
14	ALDH1L1	2.531	2.54E-05
15	BCAT1	2.452	1.10E-04
16	ITGAX	2.370	7.79E-05
17	S100A4	2.366	2.29E-03
18	LPAR3	2.353	1.56E-05
19	ITGAD	2.278	1.68E-06
20	GCSAM	2.143	1.08E-04
1	UGT1A6	-8.227	4.29E-06
2	IRF5	-5.190	3.30E-04
3	IFI44L	-2.827	1.28E-03
4	FCRL4	-2.573	2.13E-06
5	BCL2A1	-2.539	9.20E-05
6	MX1	-2.473	2.96E-04
7	IGHV1-3	-2.470	1.11E-03
8	RSAD2	-2.469	6.87E-06
9	CERK	-2.350	3.63E-03
10	AGRN	-2.326	4.26E-03
11	EPSTI1	-1.928	8.62E-04
12	OAS1	-1.857	5.94E-04
13	XAF1	-1.847	2.57E-04
14	IRF7	-1.833	3.51E-04
15	CMPK2	-1.728	8.53E-07
16	ISG15	-1.715	7.54E-05
17	H1-10	-1.706	1.23E-05
18	TIE1	-1.638	6.36E-04
19	HMGB1P3	-1.618	3.07E-03
20	OASL	-1.611	4.68E-06
DGEiT2p vs DGEZiT2p			
1	SCHIP1	6.183	1.34E-07
2	PLOD2	5.689	3.76E-08
3	CDK14	5.683	1.57E-08
4	OPHN1	5.651	1.00E-10
5	RP11-467L13	4.981	2.40E-02
6	ALDH1L1	4.187	4.18E-07
7	RNF144A	4.025	8.74E-04

8	GCSAM	2.823	1.26E-04
9	GIMAP7	2.111	1.21E-06
10	SLAMF8	2.040	1.27E-05
11	SLC39A12	2.036	8.13E-04
12	BCAT1	1.972	1.15E-03
13	PRDM16	1.903	3.52E-04
14	RHOQ	1.885	1.57E-08
15	NR4A2	1.823	6.04E-04
16	DUSP23	1.776	6.04E-04
17	TRAT1	1.720	4.18E-07
18	SMIM24	1.710	3.13E-04
19	TYROBP	1.703	2.27E-07
20	OSBPL5	1.656	2.04E-05
1	TBXAS1	-7.458	3.76E-08
2	IRF5	-6.054	5.60E-09
3	LMNA	-5.787	1.45E-06
4	PLXND1	-3.837	1.91E-05
5	AGRN	-3.627	2.50E-05
6	TSPAN33	-3.119	6.16E-05
7	IGFBP3	-3.025	3.76E-08
8	BCL2A1	-2.609	2.34E-04
9	H1-10	-2.325	3.55E-06
10	LGALS3BP	-2.304	2.82E-06
11	P2RY8	-2.082	5.00E-05
12	FCRL4	-1.979	2.41E-06
13	AIF1	-1.922	1.31E-03
14	RSAD2	-1.908	1.39E-04
15	IFI44L	-1.832	3.98E-02
16	EIF4EBP1	-1.805	3.70E-09
17	ISG15	-1.767	6.32E-05
18	TTYH3	-1.681	3.14E-07
19	PHLDA1	-1.668	4.61E-06
20	IGHV1-3	-1.626	8.43E-03
DGEiT2p vs DGE+TYR			
1	TRBV10-3	11.461	9.78E-06
2	TRAV4	10.839	6.73E-06
3	TRAJ42	7.901	1.58E-02
4	TRBJ1-3	7.478	3.72E-02
5	TYROBP	1.028	4.47E-03
1	IRF5	-2.718	2.87E-06
2	TBXAS1	-1.436	3.03E-03
3	PTAFR	-0.795	7.40E-04
DGEZiT2p vs DGEZ+TYR			
1	TRBV10-3	11.384	8.22E-06
2	TRAV4	10.782	5.93E-06
3	TRAJ42	8.251	2.67E-03
4	TRBJ1-3	7.869	4.83E-03
5	CUEDC1	1.573	4.43E-03

6	EIF4EBP1	1.295	5.93E-06
7	DMKN	1.257	3.03E-02
8	CD6	1.245	4.43E-03
9	IL10	1.179	3.79E-02
10	TCIRG1	0.949	1.23E-03
11	GSDMD	0.911	1.76E-02
12	PRDM16	0.893	2.34E-02
13	PLOD2	0.868	1.30E-02
14	GSR	0.832	3.47E-05
15	MPZL3	0.823	2.80E-05
16	DCTN6	0.815	8.31E-03
17	STK32B	0.798	2.82E-02
18	TRAC	0.795	2.97E-04
19	LY9	0.770	3.03E-03
20	SIGIRR	0.762	1.42E-02
1	XCL2	-1.126	1.17E-04
2	XCL1	-1.072	5.37E-04
3	GNLY	-0.978	1.23E-03
4	OASL	-0.966	1.38E-02
5	TNF	-0.838	3.39E-02
6	EMP3	-0.616	5.71E-03
7	NCR1	-0.515	4.53E-02
DGE+TYR vs DGEZ+TYR			
1	PLOD2	7.762	1.40E-09
2	SCHIP1	7.530	3.21E-08
3	CDK14	5.749	2.13E-08
4	OPHN1	5.580	1.40E-09
5	RNF144A	5.428	1.86E-07
6	ALDH1L1	3.985	5.66E-07
7	ITGAX	3.581	9.29E-06
8	CUEDC1	3.270	3.53E-06
9	GCSAM	2.958	1.95E-05
10	ITGAD	2.862	3.79E-07
11	PRDM16	2.687	1.26E-06
12	SLAMF8	2.656	3.79E-07
13	STK32B	2.244	7.97E-07
14	RNF122	2.079	2.33E-08
15	RP11-452L6	2.074	5.53E-06
16	GSR	2.063	1.60E-09
17	SLC39A12	2.059	9.72E-04
18	BCAT1	1.999	1.20E-03
19	UBXN8	1.971	7.64E-07
20	UBE2J1	1.861	7.00E-09
1	TBXAS1	-6.186	5.50E-06
2	IRF5	-5.431	1.42E-04
3	IGFBP3	-4.299	6.41E-08
4	LGALS3BP	-3.425	1.51E-07
5	LMNA	-3.300	6.32E-04

6	AGRN	-3.015	1.69E-04
7	FCRL4	-2.964	1.88E-07
8	IFI44L	-2.697	3.01E-03
9	ADGRG3	-2.450	4.94E-07
10	IGHV1-3	-2.260	4.02E-03
11	RSAD2	-2.224	3.25E-05
12	BCL2A1	-2.181	3.15E-03
13	CD38	-2.116	2.06E-05
14	MX1	-2.068	3.41E-03
15	TIE1	-1.790	2.65E-04
16	PHLDA1	-1.735	1.36E-05
17	ITGA1	-1.688	8.19E-07
18	OASL	-1.672	2.36E-06
19	TSPAN33	-1.655	3.49E-02
20	TUBA3C	-1.649	8.59E-06

Supplementary Table S2. Top-ranked upregulated KEGG pathways from selected CD3ζ-related comparisons that did not reach adjusted statistical significance. Analyses were performed using clusterProfiler::enrichKEGG with upregulated genes (log2FC > 0.5, FDR < 0.05). Gene Ratio indicates pathway-mapped input genes/total KEGG pathway genes; adjusted p values were Benjamini–Hochberg corrected.

Comparison	KEGG ID	Upregulated KEGG Pathway	Gene Ratio	Adj. P Value
NK-92.DGEZiT2puro vs. NK-92.iT2puro	hsa04152	AMPK signaling pathway	8/121	0.11027
	hsa04550	Signaling pathways regulating pluripotency of stem cells	8/143	0.11027
	hsa04810	Regulation of actin cytoskeleton	10/218	0.11027
	hsa05330	Allograft rejection	4/38	0.11027
	hsa05222	Small cell lung cancer	6/92	0.11027
NK-92.DGEZiT2puro vs. NK-92.DGEiT2puro	hsa04660	T cell receptor signaling pathway	7/104	0.07700
	hsa04152	AMPK signaling pathway	7/121	0.12542
	hsa04625	C-type lectin receptor signaling pathway	6/104	0.13455
	hsa04550	Signaling pathways regulating pluripotency of stem cells	7/143	0.13455
	hsa04151	PI3K-Akt signaling pathway	12/354	0.13455

Figures

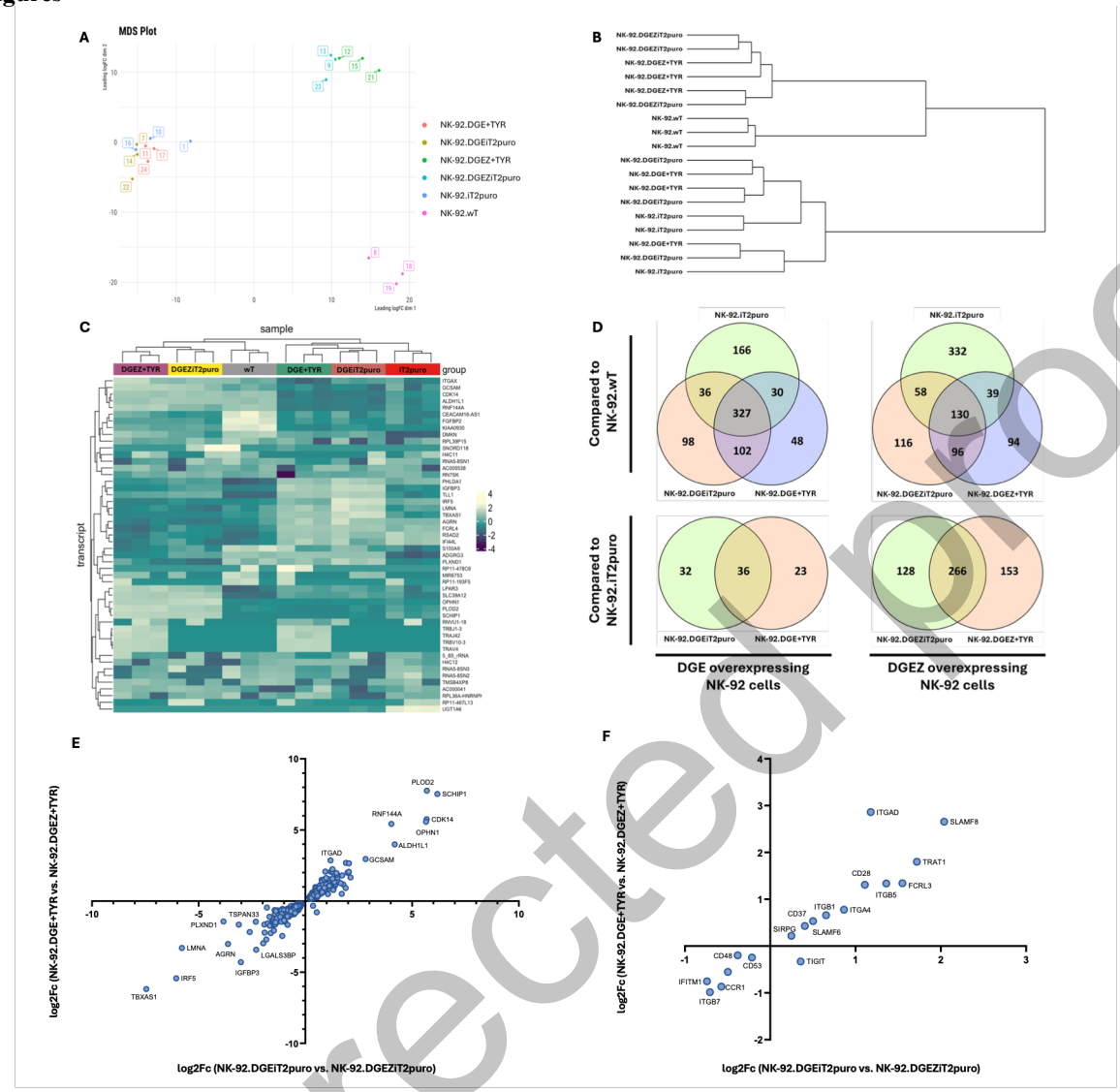

Figure 1. Global transcriptomic profiling of genetically modified NK-92 cells. (A) Multidimensional scaling plot showing overall distribution of analyzed samples. **(B)** Hierarchical clustering dendrogram. **(C)** Heatmap of the top 50 most variable transcripts across the analyzed samples. **(D)** Venn diagrams showing shared and unique differentially expressed genes (|log2FC| > 0.5, FDR < 0.05) in selected comparisons with NK-92.wT and NK-92.iT2puro cells . **(E)** Scatter plot comparing gene-level log2FC values between NK-92.DGEiT2puro vs. NK-92.DGEZiT2puro (x-axis) and NK-92.DGE+TYR vs. NK-92.DGEZ+TYR (y-axis) across all analyzed genes. Selected genes showing prominent changes are labeled. For both comparisons, positive log2FC values indicate higher expression in the second-listed, CD3ζ-overexpressing group, whereas negative values indicate higher expression in the first-listed group. **(F)** Corresponding scatter plot restricted to genes annotated as encoding cell-surface proteins based on Gene Ontology (GO) annotations obtained through the PANTHER Classification System, highlighting concordant changes in surface molecules associated with CD3ζ expression in the two engineered backgrounds.

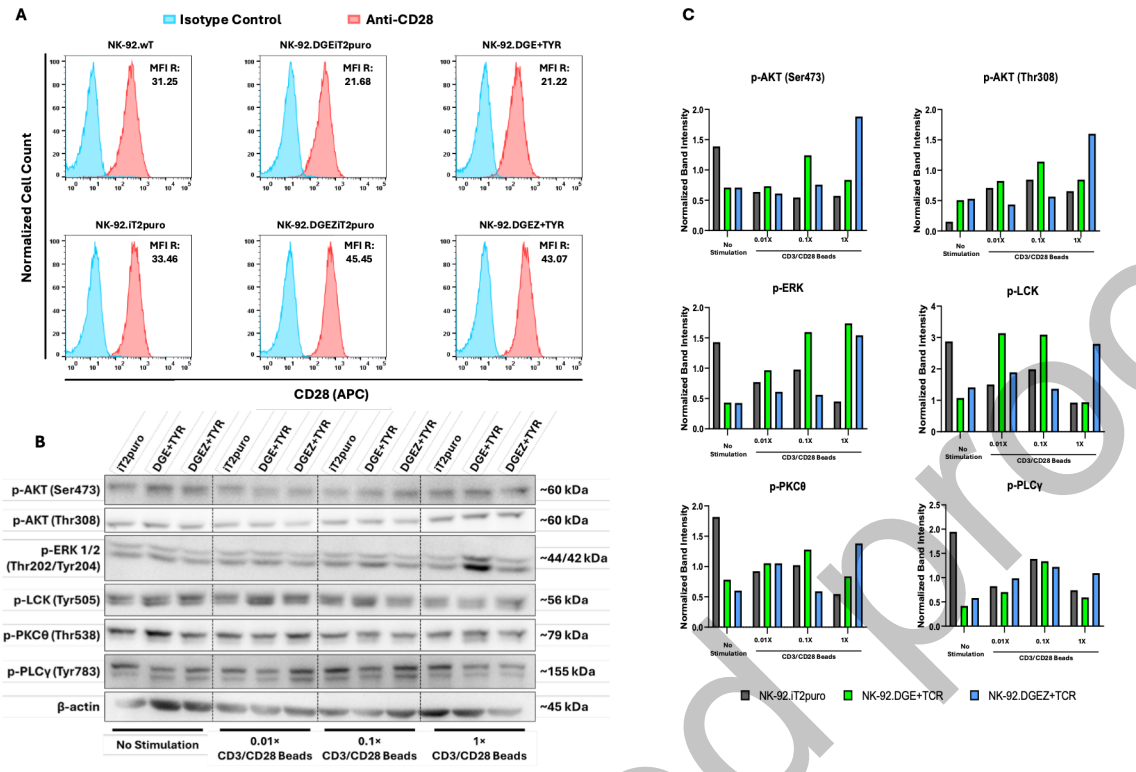

Figure 2. CD3ζ-associated phenotypic and signaling alterations in engineered NK-92 cells. (A) Analysis of surface CD28 expression by flow cytometry. MFI R: mean fluorescence intensity ratio (CD28/isotype) (B) Phospho-protein Western blots following CD3/CD28 bead stimulation (C) Densitometric quantification of Western blot results.

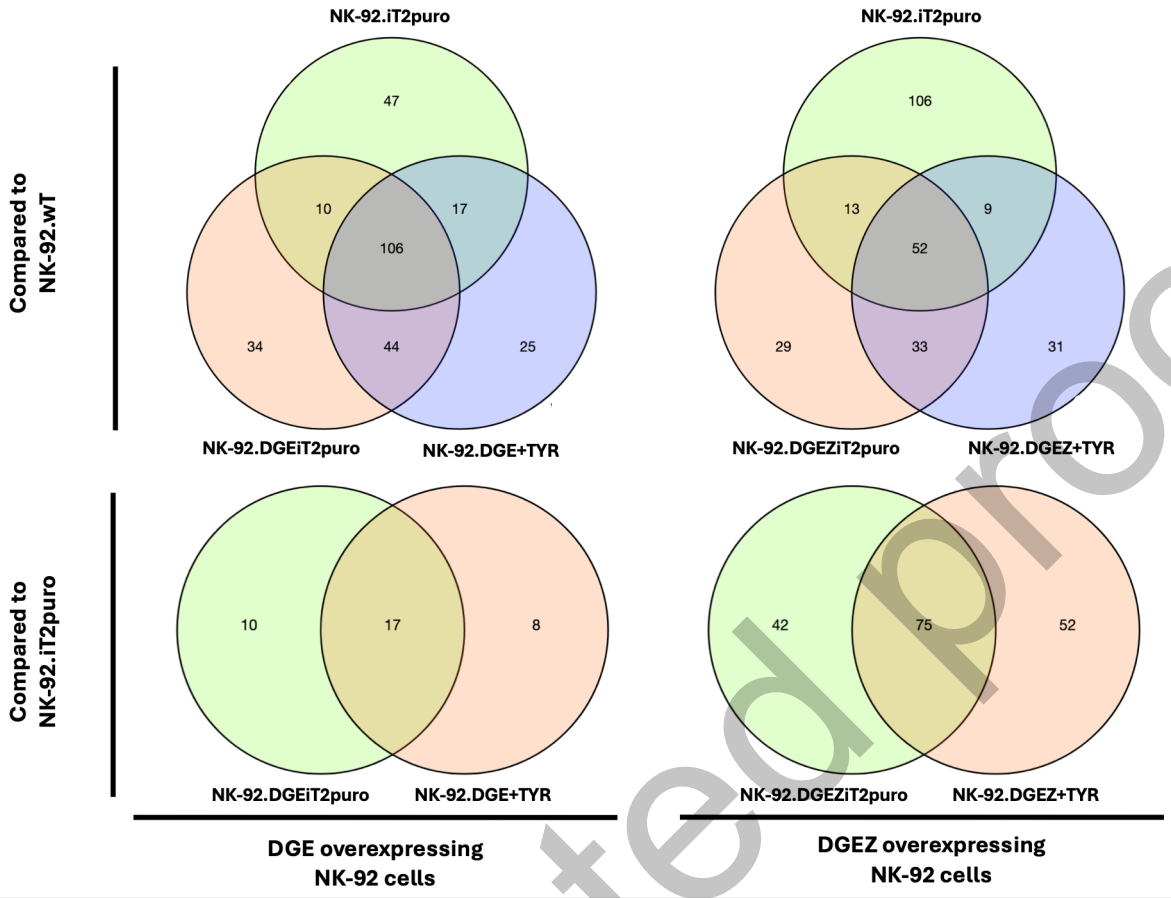

Supplementary Figure 1. Global transcriptomic profiling of genetically modified NK-92 cells using a more stringent differential-expression threshold. Venn diagrams showing shared and unique differentially expressed genes (|log2FC| > 1, FDR < 0.05) in selected comparisons with NK-92.wT and NK-92.iT2puro cells .